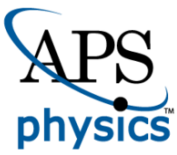

This is the accepted manuscript made available via CHORUS. The article has been published as:

Spin-Torque-Biased Magnetic Strip: Nonequilibrium Phase Diagram and Relation to Long Josephson Junctions

Daniel Hill, Se Kwon Kim, and Yaroslav Tserkovnyak

Phys. Rev. Lett. **121**, 037202 — Published 16 July 2018

DOI: 10.1103/PhysRevLett.121.037202

Spin-Torque-Biased Magnetic Strip: Nonequilibrium Phase Diagram and Relation to Long Josephson Junctions

Daniel Hill, Se Kwon Kim, and Yaroslav Tserkovnyak
Department of Physics and Astronomy, University of California, Los Angeles, California 90095, USA

Spin-torque-biased magnetic dynamics in an easy-plane ferromagnet (EPF) is theoretically studied in the presence of a weak in-plane anisotropy. While this anisotropy spoils U(1) symmetry thereby quenching the conventional spin superfluidity, we show that the system instead realizes a close analog of a long Josephson junction (LJJ) model. The traditional magnetic-field and electric-current controls of the latter map respectively onto the symmetric and antisymmetric combinations of the out-of-plane spin torques applied at the ends of the magnetic strip. This suggests an alternative route towards realizations of superfluid-like transport phenomena in insulating magnetic systems. We study spin-torque-biased phase diagram, providing analytical solution for static multidomain phases in the EPF. We adapt an existing self-consistency method for the LJJ to develop an approximate solution for the EPF dynamics. The LJJ-EPF mapping has potential for producing applications with superconductor-based circuit functionality at elevated temperatures. The results apply equally to antiferromagnets with suitable effective free energy in terms of the Néel order instead of magnetization.

Introduction.—It has been suggested [1, 2] that insulating thin-film easy-plane ferromagnets (EPF) can exhibit features of superfluid spin transport, which is attractive for spintronics applications, due to low dissipation and long-ranged signal propagation [3, 4]. However, complications can arise in that spin supercurrents, i.e., spin transport with topologically-suppressed dissipation [1], can be inhibited in an EPF by the presence of magnetic anisotropy within the easy-plane. This spoils the requisite $U(1)$ symmetry and pins the magnetization along a particular direction. Such symmetry-breaking anisotropies always exist in real materials, due to, e.g., underlying crystal symmetries or shape anisotropy, demoting the spin superfluid analogy to an imperfect one. Potential signatures of spin superfluids were recently observed in Refs. [19, 20], so measuring effects of anisotropy may be viable in the near future.

In this Letter, departing from the previous view of the EPF with in-plane anisotropy as a defective spin superfluid, we propose a description as a magnetic analog of a long Josephson junction (LJJ), which consists of two superconductors sandwiching a thin insulating layer [5]. This incorporates the in-plane anisotropy as a natural and potentially desirable ingredient. Specifically, we consider the magnetic dynamics of the EPF driven by the out-of-plane spin torques exerted at its ends. The mapping between EPF and LJJ represents a key result of the paper: Domain walls in the former correspond to phase vortices in the latter, and symmetric and antisymmetric combinations of the spin torques in the former correspond to the magnetic-field and electric-current controls of the latter.

In the following, we construct the spin-torque-biased phase diagram, in which the multivortex stationary states of the LJJ get mapped onto multi-magnetic-domain-wall stationary states in the EPF. The mapping from the equations of motion (EoM) for the LJJ to the Landau-Lifshitz-Gilbert equations for the EPF is exact for static cases, thus giving the full analytical solution for static multidomain phases in the EPF. For dynamic cases, the EoM for the EPF differ from those of the LJJ in that the dissipative leakage at the boundaries due to spin pumping [9] must be accounted for; however, techniques for approximating the dynamical solutions in LJJ's can be carried over to the EPF with minor adjustments. As an example, we develop an approximate analytical solution for the EPF dynamics by adapting an existing self-consistent method for the LJJ [8].

Magnetic model.—In this Letter, we show that a magnetic strip connected to spin-injection leads bears close analogy to a LJJ. We illustrate this by considering a simple structure depicted in Fig. 1(a). An insulating EPF of length $2L$ is subjected to spin torques $\tau_{r,l}$ applied at its left (right) interface. The underlying spin currents are injected via the spin Hall effect [10] with spins oriented out of the magnetic easy (xy) plane. The system is similar to the EPF thin-film junction of Ref. [3] but with the addition of a small in-plane anisotropy $K' \ll K$. Our magnetic free energy is given by $F[\phi, n] = \frac{1}{2}\int d^2r \left[A(\partial_{\mathbf{r}}\phi)^2 + Kn^2 + K'\sin^2\phi\right]$, where $\phi(\mathbf{r}, t)$ is the azimuthal angle of the directional (unit-vector) order parameter $\mathbf{n}(\mathbf{r}, t) \equiv (\sqrt{1-n^2}\cos\phi, \sqrt{1-n^2}\sin\phi, n)$ Its z projection, $n(\mathbf{r}, t)$, parametrizes the generator of spin rotations in the plane, which thus dictates the Poisson bracket $s\{\phi, n\} = \delta(\mathbf{r} - \mathbf{r}')$ and establishes the canonical conjugacy of the pair (ϕ, sn) [11]. s is the saturation spin density and A is the order-parameter stiffness. The hard-z-axis anisotropy $K \gg K'$ keeps the magnetization dynamics predominantly near the xy plane, which allows us to neglect the gradient terms involving n. The ground-state orientation is collinear with the x axis, according to the magnetic anisotropy $\propto K'$, dictating the presence of metastable domain-wall textures, as depicted in Fig. 1(a).

The dissipation associated with the magnetization dynamics is introduced in the conventional Gilbert-damping form [12], which for our easy-plane dynamics reduces to the Rayleigh dissipation function (per unit area) of $R = \alpha_d s(\partial_t\phi)^2/2$, parametrized by a damping constant α_d. We assume the low-bias regime, such that $|\partial_{\mathbf{r}}\phi| \ll \sqrt{K/A}$ (the Landau criterion for the stability of planar textures [1].), so as to prevent significant departures of the magnetization away from the easy plane. Thermal nucleation of magnetic vortices responsible for superfluid-like phase slips [13] is likewise neglected.

Putting these ingredients together, we obtain the EoM, $s\partial_t\phi = Kn$ and $s\partial_t n = A\partial_{\mathbf{r}}^2\phi - \frac{K'}{2}\sin 2\phi - \alpha_d s\partial_t\phi$. Boundary conditions are set by spin injection/pumping. The total out-of-plane spin-current densities through the right (left) interface, in the positive x direction are [3]

$$j_{r,l}^{(s)} = \mp\frac{g}{4\pi}\left[\mu_{r,l}^{(s)} - \hbar\partial_t\phi\right], \tag{1}$$

where g is the (real part of) the spin-mixing conductance per unit length of the interface and $\mu^{(s)}$ is the out-of-plane spin accumulation near the interface, which is induced by the spin Hall effect in the metal contacts. For the sake of simplicity, we assume the spin-mixing conductances to be the same for both interfaces. Recognizing the stiffness $\propto A$ term in the EoM as stemming from the bulk spin current $\mathbf{j}^{(s)} = -A\partial_{\mathbf{r}}\phi$, so that $s\partial_t n = -\partial_{\mathbf{r}}\cdot\mathbf{j}^{(s)} + \ldots$ [1], we invoke spin continuity to obtain the boundary conditions:

$$-A\partial_x\phi(\pm L,t) = j_{r,l}^{(s)} = \tau_{r,l} \pm \gamma\partial_t\phi(\pm L,t)\,. \tag{2}$$

Here, $\tau_{r,l} \equiv \mp\frac{g}{4\pi}\mu_{r,l}^{(s)} = \frac{\hbar\tan\theta_{\rm SH}}{2e}j_{r,l}$ is the spin Hall torque at the left (right) interface generated by an electric current density $j_{r,l}$ flowing in the y direction through the metal leads. $\theta_{\rm SH}$ is the effective spin Hall angle of the interfaces [14]. $\gamma \equiv \hbar g/4\pi$ parametrizes spin pumping out of the ferromagnet by the magnetic dynamics [9].

Eliminating n from the EoM and applying the substitution

$$\tilde\phi = 2\phi\,, \tag{3}$$

we arrive at the damped sine-Gordon equation:

$$\partial_x^2\tilde\phi = \frac{\partial_t^2\tilde\phi}{u^2} + \frac{\sin\tilde\phi}{\lambda^2} + \beta_d\partial_t\tilde\phi\,, \tag{4}$$

with the wave speed $u = \sqrt{AK}/s$, characteristic domain-wall width $\lambda = \sqrt{A/K'}$, and damping constant $\beta_d = \alpha_d s/A$. This equation admits a solution of an isolated domain wall as well as low-amplitude spin-wave solutions which obey the massive Klein-Gordon equation, with the mass proportional to K'. In the large spin-current limit, so that $|\partial_{\mathbf{r}}\phi| \gg 1/\lambda$, the excitations become approximately massless. In this (linearly-dispersing) limit, the system approaches the behavior of the EPF without in-plane anisotropy, thus allowing for states that closely resemble the spin superfluid of Ref. [3]. In the small spin-current regime, on the contrary, the steady state configuration is static, laking the aforementioned spin-superfluid dynamics, but the analogy to LJJ nevertheless holds.

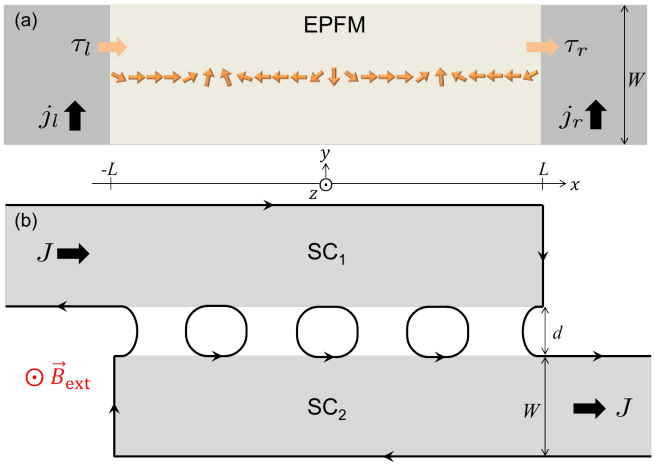

FIG. 1. (a) EPF with spin injection from metal contacts on two side. The spin polarization of the current is along the z axis, while the spin-current flow is oriented along the x axis. The ferromagnet is sufficiently narrow in the transverse dimensions to treat it as quasi-one-dimensional. (b) Diagram of the inline LJJ, with W much smaller than L as well as the depth of the structure in the z direction. We assume two conventional superconductors (SC) much larger than the London penetration depth in all dimensions. The magnetic-field screening currents as well as the circulating vortices are schematically depicted with black oriented lines. The vortices in the junction map onto the domain walls depicted in (a).

The damped sine-Gordon equation has found application in a number of disciplines [15]. The equation is commonly studied in relation to its physical realizations in coupled series of pendulums and long Josephson Junctions. Below we exploit some relevant results of the latter.

Relation to long Josephson junctions.—It is instructive to recall the dynamics of the inline configuration of a LJJ [16, 17], a diagram of which is depicted in Figure 1(b). A Josephson junction permits coherent supercurrent tunneling through the insulating region up to a critical current density j_c, which depends on the tunneling strength and the superfluid density in the superconductor. In the presence of a magnetic field $\mathbf{B} = B(x)\mathbf{z}$ inside of the junction, we can choose a gauge $\mathbf{A} = A(x,y)\mathbf{x}$, so that $B = -\partial_y A$. The DC Josephson relation for the tunneling current flowing from SC$_1$ to SC$_2$ is

$$j = j_c\sin\vartheta + gV\,, \tag{5}$$

where $\vartheta(x) = \theta_1 - \theta_2$ is the superconducting phase difference across the junction, and we also added the normal current component proportional to the conductance (per

unit area) g and the local voltage $V(x) = V_1 - V_2$ across the junction. $B(x)$ satisfies the Ampère-Maxwell equation

$$\partial_x B = \frac{4\pi}{c} j + \frac{\varepsilon}{c}\partial_t E\,, \tag{6}$$

where $E = -\mathbf{E}\cdot\mathbf{y} = V/d$ is the electric field in and ε the permittivity of the insulating region.

Next, we invoke the superconducting phase evolution equation ($e > 0$)

$$V = \frac{\hbar}{2e}\partial_t \vartheta \tag{7}$$

and the relation $\partial_x \theta = -(2e/\hbar c)A$ well inside of the superconducting regions (on the scale of the London penetration depth λ_L), which leads to

$$B = \frac{A_2 - A_1}{d + 2\lambda_L} = \frac{\hbar c}{2e(d+2\lambda_L)}\partial_x \vartheta\,. \tag{8}$$

Putting Eqs. (5)-(8) together, we reproduce the damped sine-Gordon equation (4), thus identifying the Swihart velocity $u = c\sqrt{\frac{d}{\varepsilon(d+2\lambda_L)}}$, the Josephson penetration depth $\lambda_J = c\sqrt{\frac{\hbar}{8\pi e(d+2\lambda_L)j_c}}$, and the damping parameter $\beta_d = \frac{4\pi g(d+2\lambda_L)}{c^2}$.

The boundary conditions are obtained from Eq. (8) by noting that

$$B(\pm L) = B_{\rm ext} \pm \frac{2\pi}{c} J\,, \tag{9}$$

where $B_{\rm ext}$ is the externally applied field in the z direction and J is the applied current through the system, per unit of length in the z direction. Comparing this with Eq. (2), we see that the symmetric (antisymmetric) combination of the torques, $\tau_r \pm \tau_l$, realizes the effect of the external field $B_{\rm ext}$ (applied current J), in the mapping from the LJJ to the EPF:

$$\frac{\tau_{r,l}}{A} \rightleftharpoons -\frac{e}{\hbar c}(d+2\lambda_L)\left(B_{\rm ext} \pm \frac{2\pi}{c} J\right)\,. \tag{10}$$

The EoM of the LJJ and anisotropic EPF systems differ only in the addition of the boundary spin pumping term, $\gamma\partial_t\phi$, in Eq. (2). If spin pumping is negligible, e.g. time-independent solutions, the two problems are equivalent. Having an exact mapping between the models of the LJJ and EPF for time-independent solutions allows the equilibrium stability analysis of Ref. [6] to carry over. The close analogy of the EPF system to the thoroughly studied LJJ model allows us to immediately draw several conclusions about the static solutions. The substitution (3) indicates that a 2π phase vortex in the LJJ model corresponds to a domain wall (π rotation) in the EPF. In particular, the symmetric torque $\tau_r = \tau_l$ injects static domain-wall textures into the EPF, which in the LJJ corresponds to the external field $B_{\rm ext}$ producing a static multivortex configuration. The number of stable domain walls is dependent on the boundary conditions and the solution for a given boundary condition can be multivalued, resulting in hysteretic effects. The multivalued solutions are dependent on the length of the system, in units of λ. Figure 2 shows the regions of stability for p-vortex equilibrium solutions for the case of $L = \lambda$. The stability regions have greater overlap in the limit of large L/λ, and in this limit the edge of the $p > 0$ stability region asymptotically approaches the zero bias point as $\sim e^{-L/p\lambda}$. See Ref. [6] for the analytic equations for computing the phase boundaries.

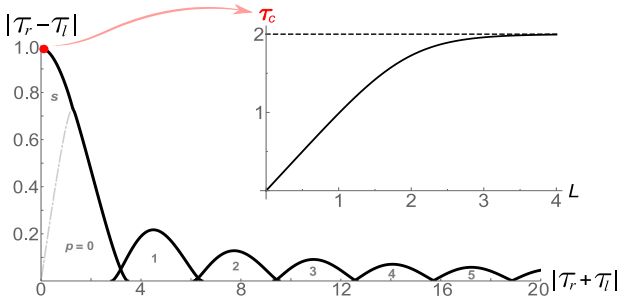

FIG. 2. The regions of stability for equalibium p-vortex solutions of the LJJ boundary-value problem, for $L/\lambda = 1$. The spin torques $\tau_{r,l}$ are in units of A/λ. Overlapping regions can have either solution. Outside of these regions, i.e., in the high $|\tau_r - \tau_l|$ limit, there are no stable time-independent solutions. Inset: The dependence of the critical torque τ_c, for which $\tau_r + \tau_l = 0$, on the length L in units of λ.

Analytic equilibrium solutions.—Using the stable solutions of the LJJ problem studied in Ref. [6], we map back to the EPF to find the static domain-wall configurations. We give the form of the $\phi(x)$ solutions after mapping to the EPF, as well as some general remarks, and refer to Refs. [6, 7] for further details. Similar solutions were recently found for the one terminal case in Ref. [18]. From the p-vortex LJJ solutions, we find p-domain-wall solutions in the EPF have the form

$$\phi(x) = \eta \begin{cases} \frac{\pi}{2}(p-1) + \mathrm{am}\left(\xi + K(k), k\right)\,, & \text{for } p \text{ even} \\ \frac{\pi}{2}p + \mathrm{am}\left(\xi, k\right)\,, & \text{for } p \text{ odd} \end{cases}\,, \tag{11}$$

where $\xi = \frac{x}{k\lambda} + \alpha$, and $\eta = \pm 1$ for $\tau_r + \tau_l \lessgtr 0$. Here, α and k are parameters determined by the boundary conditions, and $\mathrm{am}(u)$ and $K(u)$ are the Jacobi amplitude function and complete elliptic integral of the first kind, respectively.

The zero-domain-wall region includes a portion, separated by the gray line and labeled by s in Fig. 2, in which Eq. (11) no longer holds. The solution in the s region has the form

$$\phi(x) = \zeta \cos^{-1}\left[k\frac{\mathrm{cn}\left(x/\lambda + \beta\right)}{\mathrm{dn}\left(x/\lambda + \beta\right)}\right]\,, \tag{12}$$

where k and β are again determined by the boundary conditions, $\zeta = \pm 1$ for $\tau_r - \tau_l \lessgtr 0$, and $\mathrm{cn}(u)$ and $\mathrm{dm}(u)$ are the Jacobi elliptic cosine and delta amplitude, respectively. In the case of $L = \infty$, the s crossover line becomes a phase-transition line from a no-domain-wall phase to a many-domain-wall phase, but away from this limit the crossover from s to $p = 0$ is smoothed out by finite-size effects and no phase transition takes place.

In the special case of perfectly asymmetric boundary conditions, i.e., $\tau_r = -\tau_l$, the equilibrium solution is given by Eq. (12) with $\beta = 0$, up to the critical value of $|\tau_r - \tau_l| \to \tau_c$. This critical asymmetric torque τ_c is analogous to the critical current J_c in the LJJ model, with, as shown in the Fig. 2 inset, its value depending on the normalized length of the system. τ_c approaches A/λ asymptotically as $L \to \infty$ and diminishes as $\tau_c = LK'$ for $L \to 0$. For yttrium iron garnet, $A \sim 10^{-11}$ J/m^2, so the saturated critical torque (per unit area), corresponding to $\lambda \sim 100$ nm would be $A/\lambda \sim 10^{-4}$ J/m^2. Using the spin Hall angle $\theta_{\mathrm{SH}} \sim 0.1$, the corresponding electrical current density needed at the metallic contacts in order to approach τ_c is of order 10^{12} A/m^2, which is high but feasible.

Dynamic solutions.—Here, inspired by the LJJ analogy, we apply a method similar to that of Ref. [8] in finding an approximate dynamic, spin-propagating solution for the EPF EoM, Eq. (4) with boundary conditions (2). To simplify the discussion, we adopt dimensionless notation, such that $A = u = \lambda = 1$. It is natural to start with a trial solution of the form $\tilde{\phi}(x,t) = \Omega t + f(x) + \epsilon(x,t)$. where $\epsilon(x,t)$ is a small periodic function with the to-be-determined period $T = 2\pi/\Omega$ and with zero time average, and $f(x)$ is a to-be-determined time-independent function. We consider the weak in-plane anisotropy limit for which $\epsilon(x,t) \ll 1$. The boundary conditions are

$$-\partial_x f(\pm L) = 2\tau_{r,l} \pm \gamma\Omega \tag{13}$$

and

$$\partial_x \epsilon(\pm L, t) = 0\,, \tag{14}$$

where we discard the boundary term $\gamma\partial_t\epsilon$ by considering the $\gamma \ll 1$ limit[21]. Plugging the trial solution into Eq. (4) and averaging over the period T, denoted by $\langle \ldots \rangle_T$, we get the time-independent equation $\partial_x^2 f = \beta_d\Omega + \langle \sin\tilde{\phi} \rangle_T$. Integrating and applying the boundary conditions, we find the self-consistency equation

$$f(x) = \int_{-L}^{x} dx_1 \int_{-L}^{x_1} dx_2 \left[\beta_d\Omega + \langle \sin\tilde{\phi} \rangle_T(x_2)\right] - (2\tau_l - \gamma\Omega)x\,, \tag{15}$$

with the constraint

$$\int_{-L}^{L} dx \langle \sin\tilde{\phi} \rangle_T = 2(\tau_l - \tau_r - \gamma\Omega - L\beta_d\Omega)\,. \tag{16}$$

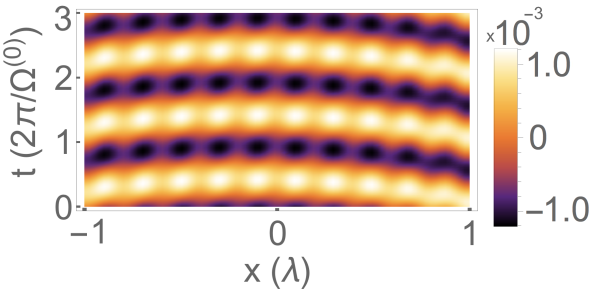

FIG. 3. Plot of the approximate modulation of the superfluid phase solution, $\epsilon^{(0)}(x,t)$, resulting from a weak in-plane anisotropy, with $L = 1$, $\beta_d = 0.1$, $\gamma = 0.01$, $\tau_l = 1.5$, and $\tau_r = -2$.

Note that the integral on the right-hand side of Eq. (15) depends on both $f(x)$ and $\epsilon(x,t)$ through $\tilde{\phi}$.

For the time-dependent part of the solution, the dominant contribution is harmonic in Ωt and obeys $\partial_x^2\epsilon - \partial_t^2\epsilon - \beta_d\partial_t\epsilon = \sin(\Omega t + f)$. The solution satisfying the boundary conditions (14) is then readily found to be

$$\epsilon(x,t) = \mathrm{Im}\Big(\frac{e^{i\Omega t}}{2i\omega}\big[e^{i\omega x}F^-(x) - e^{-i\omega x}F^+(x) + A\cos(\omega x + \omega L)\big]\Big)\,, \tag{17}$$

where $A = i\left[e^{i\omega L}F^-(L) + e^{-i\omega L}F^+(L)\right]/\sin(2\omega L)$, $\omega^2 = \Omega^2 - i\beta_d\Omega$, and the functions $F^{\pm}(x) = \int_{-L}^{x} dx_1\, e^{if(x_1)\pm i\omega x_1}$. Equations (15), (16), and (17) form a system of coupled integral equations for $f(x)$, Ω, and $\epsilon(x,t)$. Approximate solutions can be found iteratively by starting with, for example, $\langle \sin\tilde{\phi} \rangle_T^{(0)} = 0$, which implies $f^{(0)}(x) = \beta_d\Omega^{(0)}(x+L)^2/2 - (2\tau_l - \gamma\Omega^{(0)})(x+L)$, with $\Omega^{(0)} = (\tau_l - \tau_r)/(L\beta_d + \gamma)$. This agrees with the XY-model solution [22] of Ref. [4]. This intermediate solution can be plugged into Eq. (17) to get $\epsilon^{(0)}(x,t)$, an example of which is plotted in Fig. 3. These in turn can be used to evaluate $\langle \sin\tilde{\phi} \rangle_T^{(1)}$ for generating a new set $f^{(1)}(x)$, $\Omega^{(1)}$, and $\epsilon^{(1)}(x,t)$, and so on.

Note that the frequency of oscillation of the superfluid phase, Ω, is modulated as a function of EPF length, L, as a result of the in-plane anisotropy. This is seen through the dependence of Ω on the integral on the right-hand side of Eq. (16). The predicted dependence of Ω on L can in practice provide a useful experimental probe of the underlying physics.

Because the transmitted superfluid current is dependent on Ω, this modulation effect could in principle be measured by injecting sufficient spin current ($\tau \gtrsim A/\lambda$) into insulating thin film ferromagnets of variable length and measuring the inverse spin Hall effect on the opposite end, using similar methods to those discussed in Refs. [23, 24].

Discussion.—Given that Josephson junction systems have many potential uses as computing circuit elements,

e.g. as a transistor[25] or memristor[26], the close analogy between the EPF and LJJ suggests a potential for similar spintronic applications which could operate in much the same manner as the proposed LJJ devices, due to the vortex/domain-wall corespondence between the systems, thus taking advantage of the history-dependence and information storage potential of the domain walls. Such EPF-based devices would use currents through the spin Hall contacts as inputs and would produce an output either by measuring the inverse spin Hall voltages resulting from a change of state, e.g. injection of a domain wall, or by directly reading the number of domain walls, which is possible with e.g. the magneto-optical Kerr effect[27] or magnetic force microscopy[28]. Using EPF-based spintronics devices instead of LJJ-based superconducting devices as building blocks of circuit elements could have practical advantages, e.g. the relevant physics such as the spin Hall torque[29] being able to operate at room temperature and the use of eletrical current inputs instead of precisely controlled magnetic fields to control the state of the system.

We wish to thank the anonymous referees, whose comments and questions led to the significant improvement of the Letter. This work was supported by the Army Research Office under Contract No. W911NF-14-1-0016.

[1] E. B. Sonin, Sov. Phys.–JETP **47**, 1091 (1978); Adv. Phys. **59**, 181 (2010).
[2] J. König, M. C. Bønsager, and A. H. MacDonald, Phys. Rev. Lett. **87**, 187202 (2001).
[3] S. Takei and Y. Tserkovnyak, Phys. Rev. Lett. **112**, 227201 (2014).
[4] S. Takei and Y. Tserkovnyak, Phys. Rev. Lett. **115**, 156604 (2015).
[5] C. S. Owen and D. J. Scalapino, Phys. Rev. **164**, 538 (1967).
[6] S. V. Kuplevakhsky and A. M. Glukhov, Phys. Rev. B. **76**, 174515 (2007).
[7] S. V. Kuplevakhsky and A. M. Glukhov, Phys. Rev. B. **73**, 024513 (2006).
[8] M. Jaworski, Supercond. Sci. Technol. **21**, 065016 (2008).
[9] Y. Tserkovnyak, A. Brataas, and G. E. W. Bauer, Phys. Rev. Lett. **88**, 117601 (2002).
[10] J. Sinova, S. O. Valenzuela, J. Wunderlich, C. H. Back, and T. Jungwirth, Rev. Mod. Phys. **87**, 1213 (2015).
[11] B. I. Halperin and P. C. Hohenberg, Phys. Rev. **188**, 898 (1969).
[12] T. L. Gilbert, **40**, 3443 (2004).
[13] S. K. Kim, S. Takei, and Y. Tserkovnyak, Phys. Rev. B **93**, 020402(R) (2016).
[14] Y. Tserkovnyak and S. A. Bender, Phys. Rev. B **90**, 014428 (2014).
[15] J. Cuevas-Maraver, P. Kevrekidis, and F. Williams, eds., *The sine-Gordon Model and its Applications*, Nonlinear Systems and Complexity, Vol. 10 (Springer, Cham, 2014).
[16] R. Gross, A. Marx, and F. Deppe, *Applied Superconductivity: Josephson Effect and Superconducting Electronics*, de Gruyter Textbook (Walter De Gruyter Incorporated, 2016).
[17] R. Parmentier, in *The New Superconducting Electronics. NATO ASI Series*, Vol. 251, edited by H. Weinstock and R. Ralston (Springer, Van Godewijckstraat 30, 3311 GX Dordrecht, Netherlands, 1993) Chap. 7, pp. 221–248.
[18] E. Iacocca, T. J. Silva, and M. A. Hoefer, Phys. Rev. B **96**, 134434 (2017).
[19] W. Yuan, Q. Zhu, T. Su, Y. Yao, W. Xing, Y. Chen, Y. Ma, X. Lin, J. Shi, R. Shindou, X. C. Xie, and W. Han, Sci. Adv. **4** (2018), eaat1098.
[20] P. Stepanov, S. Che, D. Shcherbakov, J. Yang, K. Thilahar, G. Voigt, M. W. Bockrath, D. Smirnov, K. Watanabe, T. Taniguchi, R. K. Lake, Y. Barlas, A. H. MacDonald, and C. N. Lau, arXiv:1801.07290.
[21] This approximation is made to simplify the discussion. Without this constraint, ϵ satisfies $\partial_x\epsilon \pm \gamma\partial_t\epsilon = 0$ at the right (left) boundary, and the resulting solution is similar but lengthier than the one presented here.
[22] Note that our definitions of Ω and L, chosen to more closely adhere to the LJJ references, differ from Ref. [4] by a factor of 2.
[23] Y. Kajiwara, K. Harii, S. Takahashi, J. Ohe, K. Uchida, M. Mizuguchi, H. Umezawa, H. Kawai, K. Ando, K. Takanashi, S. Maekawa, and E. Saitoh, Nature **464**, 262 (2010).
[24] H. Chen, A. D. Kent, A. H. MacDonald, and I. Sodemann, Phys. Rev. B **90**, 220401 (2014).
[25] G. P. Pepe, R. Scaldaferri, L. Parlato, G. Peluso, C. Granata, M. Russo, G. Rotoli, and N. E. Booth, Supercond. Sci. Technol. **14**, 987 (2001).
[26] C. Guarcello, P. Solinas, M. Di Ventra, and F. Giazotto, Sci. Rep. **7** (2016).
[27] G. S. D. Beach, C. Nistor, C. Knutson, M. Tsoi, and J. L. Erskine, Nature Materials **4**, 741 (2005).
[28] S. S. P. Parkin, M. Hayashi, and L. Thomas, Science **320**, 190 (2008).
[29] I. M. Miron, K. Garello, G. Gaudin, P.-J. Zermatten, M. V. Costache, S. Auffret, S. Bandiera, B. Rodmacq, A. Schuhl, and P. Gambardella, Nature **476**, 189 (2011).